

ACCEPTED VERSION

Alexander B. Sturm, Phillip Visintin, Deric J. Oehlers

Blending fibres to enhance the flexural properties of UHPFRC beams

Construction and Building Materials, 2020; 244:1-17

© 2020 Elsevier Ltd. All rights reserved.

This manuscript version is made available under the CC-BY-NC-ND 4.0 license

<http://creativecommons.org/licenses/by-nc-nd/4.0/>

Final publication at: <http://dx.doi.org/10.1016/j.conbuildmat.2020.118328>

PERMISSIONS

<https://www.elsevier.com/about/policies/sharing>

Accepted Manuscript

Authors can share their [accepted manuscript](#):

24 Month Embargo

After the embargo period

- via non-commercial hosting platforms such as their institutional repository
- via commercial sites with which Elsevier has an agreement

In all cases [accepted manuscripts](#) should:

- link to the formal publication via its DOI
- bear a CC-BY-NC-ND license – this is easy to do
- if aggregated with other manuscripts, for example in a repository or other site, be shared in alignment with our [hosting policy](#)
- not be added to or enhanced in any way to appear more like, or to substitute for, the published journal article

1 March 2024

<http://hdl.handle.net/2440/125027>

BLENDING FIBRES TO ENHANCE THE FLEXURAL PROPERTIES OF UHPFRC BEAMS

¹Sturm, A.B., ²Visintin, P., ³Oehlers, D.J.

Construction and Building Materials [Volume 244](#), 30 May 2020, 118328

<https://doi.org/10.1016/j.conbuildmat.2020.118328>

ABSTRACT

In this paper, the flexural behaviour of ultra-high performance fibre reinforced concrete (UHPFRC) beams reinforced with macro-, micro- and a blend of macro- and micro-fibres is investigated at all limit states. The goal of this study is to investigate whether the benefits of fibre blending that are observed at a material scale translate to the structural scale. To this end, six UHPFRC beams with two different cross-sections and three different mix designs were tested. Standard codified approaches as well as a segmental analysis technique are then applied to predict the measured load-deflection and load-crack width behaviour of the beams and it is shown that while standard approaches can predict serviceability deflections, the segmental analysis is more accurate when predicting crack width, member ductility and ultimate deformations. Following validation for beams with blended fibres, it is then used as the basis for a parametric study to further investigate the influence of beam geometry and reinforcing details.

KEYWORDS: fibre reinforced concrete; UHPC; UHPFRC; blended fibres; deflection; crack width; ductility

1. INTRODUCTION

The introduction of steel fibres into a cementitious matrix allows the transfer of stresses across fractures in the material and, therefore, improves material ductility in both compression and

tension [1]. At a structural level, this improvement in material performance translates to a reduction in deflections and crack widths at the serviceability limit [2], and an increase in strength and ductility at the ultimate limit [3]. The substantial benefits arising from the addition of fibres to concrete and mortars has made it a focus of significant recent research efforts; particularly in the case of ultra-high performance fibre reinforced concrete (UHPFRC) which is generally characterised by strengths of greater than 150 MPa and a high fibre content that allows non-negligible tensile stresses to be developed post-cracking.

A vast array of steel fibres with different shapes and sizes are now available commercially [4]. Extensive research at a material level has explored the potential benefits of blending multiple types of steel fibre within a given normal- or high- strength concrete mix [5-12] and to a lesser extent in UHPFRC [13-18]. A summary of the types of fibres blended and the impact on performance is summarised in Table 1 in which it is shown that there is a general consensus that hybridising fibres result in greater ductility in tension, and that substituting micro-fibres for macro-fibres improves the properties of the material.

Table 1: Summary of works on fibre blending at a material level

Reference	f_c	V_f (%)	Test	Macro-fibre	Micro-fibre	Findings
Sun et al. [5]	^a	1.5	Shrinkage, Water Permeation Flexural	35/0.43 ^b	10/0.2, 5/0.1 ^b	Micro-fibres decreased shrinkage and reduced permeation height
Lawler et al. [6]	^c	0.5-1	Tension, Direct Tension Flexural	Hooked 30/0.5	Straight 6/0.022	^d
Sorelli et al. [7]	29-33	0.38	Tension, Direct Tension	30/0.6 ^b	12/0.18 ^b	Improvement at both large and small crack widths from using hybrid fibres
Markovic [8]	113-134	1-3	Flexural Tension,	Hooked 40/0.5,	Straight 13/0.2	^d

			Direct Tension	Hooked 60/0.7		
Banthia & Sappakitti pakorn [9]	34- 39	0.5- 0.75	Flexural Tension	Crimped 30/0.8	Crimped 30/0.45, Crimped 30/0.4	Mixes with thinner fibres had improved performance
Stahli & van Mier [10]	139	6	Flexural Tension, Flowability	Crimped 30/0.6	Straight 12/0.2, Straight 6/0.15	e
Kim et al. [13]	200	1-2.5	Flexural Tension	Straight 30/0.3, Hooked 30/0.38, Hooked 62/0.78, Twisted 30/0.3	Straight 13/0.2	Hybrid mixes had larger deflections and greater toughness at the peak strength
Akcay & Tasdemir [11]	115- 124	0.75- 1.5	Flexural Tension, Splitting Tension	Hooked 30/0.55	Straight 6/0.15	e
Akcay [12]	130- 134	3-5	Direct Tension	12/0.2 ^b	6/0.15 ^b	d
Park et al. [14]	200	1-2.5	Direct Tension	Straight 30/0.3, Hooked 30/0.38, Hooked 62/0.78, Twisted 30/0.3	Straight 13/0.2	d
Nguyen et al. [15]	170- 210	1.5-2	Flexural Tension	Twisted 30/0.3	Straight 13/0.2	e
Visintin et al. [16]	150- 160	2.85	Direct Tension, Tension Stiffening	Hooked 35/0.55	Straight 13/0.2	Hybrid mixes had greater ductility than the single fibre mixes
Fantilli et al. [17]	182	0.5-3	Direct Tension	Hooked 30/0.38	Straight 6/0.16	d
Chun & Yoo [18]	190	2	Fibre Pullout, Direct Tension	Straight 30/0.3, Hooked 30.0.375, Twisted 30/0.3	Straight 13/0.2	Replacing macro-fibres with micro-fibres increased the post- cracking tensile strength and fracture energy for the mixes with hooked and twisted fibres

^a fc unknown, w/cm=0.32

^b geometry unknown

^c f_c unknown, $w/c=0.45$

^d V_f varied between the hybrid and control mixes

^e Did not include control mixes

Despite the favourable results observed at the material level, investigations on the benefit of fibre blending at the member level are much more limited, with the only studies identified being that of Voo et al. [19] and Turker et al. [20]. Voo et al. [19] tested a single beam failing in shear that contained a blend of micro- and hooked end macro-fibres. The results of this study were in contrast to those obtained at a material level because it was observed that a reduction in performance occurred as a result of fibre blending. Turker et al. [20] tested 12 UHPFRC beams in flexure with either no fibres, micro fibres or a blend of macro and micro fibres. They found an increase in ultimate deflection and a reduction in peak load when using a blend of macro and micro fibres, however, as they did not test a series with only macro fibres it cannot be determined whether the changes were due to the increasing volume of macro fibres or due to hybridisation. On a smaller scale, Visintin et al. [16] tested 5 different blends of macro- and micro-fibres to investigate the influence of fibre blending on tension stiffening prisms. It was observed, in this study, that tension stiffening was improved by the blending of fibres and that the overall best performance resulted from a 50:50 blend of macro- and micro- fibres.

The focus of this paper is the further examination of the performance of UHPFRC with blended macro- and micro-fibres by now considering the performance of flexural elements. To this end, six UHPFRC beams with two different cross sections and three different mix designs (100% macro-fibres, 100% micro-fibres and, 50% macro-fibres and 50% micro-fibres) were tested. The experimental load-deflection and load-crack width results are then compared to the predictions obtained using code approach methods and a segmental analysis for which variants

of differing complexity have been developed by Bachman [21], Bigaj [22], Schumacher [1], and Visintin & Oehlers [23]. Finally having validated the application of the segmental approach to mixes with blended fibres, a parametric study is conducted to further extend the investigation to beams with different depths and reinforcement ratios.

2. MATERIALS

The UHPFRC used for the manufacture of all test specimens was developed at the University of Adelaide by Sobuz et al. [24]. The mix design is summarised in Table 2 and is based on the use of a blended binder consisting of a sulphate-resisting cement and silica fume, a washed river sand with a fineness modulus of 2.34, and a third-generation high range water reducing superplasticiser. In all mixes, the total fibre volume has been fixed at 2.8% and the type of fibre has been varied. The macro-fibres are 35 mm long hooked end fibres with an aspect ratio of 65, while the micro-fibres are straight with a length of 13 mm long and an aspect ratio of 65. The macro-fibres have a yield strength of 1100 MPa and the micro-fibres had a yield strength of 2850 MPa. Note that these mixes are a subset of those previously used by the authors to quantify the impact of fibre blending on the tensile [16], bond [25] and shear friction [26] behaviour of UHPFRC.

Table 2: Mix Design

Mix	Unit Weight (kg/m ³)		
	1M:0m ^a	0M:1m	0.5M:0.5m
Cement	950	950	950
Superplasticiser	43	43	43
Water	168	168	168
Silica Fume	253	253	253
Fine Aggregate	943	943	943
Macro-fibres	221	0	111
Micro-fibres	0	221	111

^a0.5M:0.5m refers to a mixture with 50% macro fibres (M) and 50% micro fibres (m)

Table 3: Material properties for each mix

	1M:0m	0M:1m	0.5M:0.5m
Compressive Strength (MPa)	146	150	128
Elastic Modulus (GPa)	43.9	39.7	36.5
Shrinkage Strain At testing of beam section ($\mu\epsilon$)	434 (40 days)	439 (34 days)	475 (28 days)
	At testing of slab section	452 (49 days)	475 (41 days)
			499 (33 days)

The material properties for each mix are summarised in Table 3: the compressive strength is the average of three tests on 100 mm x 200 mm cylinders in accordance with AS1012.9:2014 [27]; the elastic modulus was obtained from tests on identical cylinders in accordance with AS1012.17-1997 [28]; and the shrinkage strain was obtained from tests conducted on prismatic sections with a cross section of 75 mm x 75 mm and a length of 285 mm and which were subjected to the same conditions as the beam specimens and tested in accordance with AS1012.13:2015 [29]. The full compressive stress strain behaviour is shown in Fig. 1(a) in which compressive stresses and strains are shown as negative. The remaining material properties required for analysis, including the tensile stress-crack width relationship in Fig. 1(b) and the concrete bond stress-slip behaviour in Fig. 1(c), are taken from Visintin et al. [16] and Sturm & Visintin [25] where the same mix designs have been used.

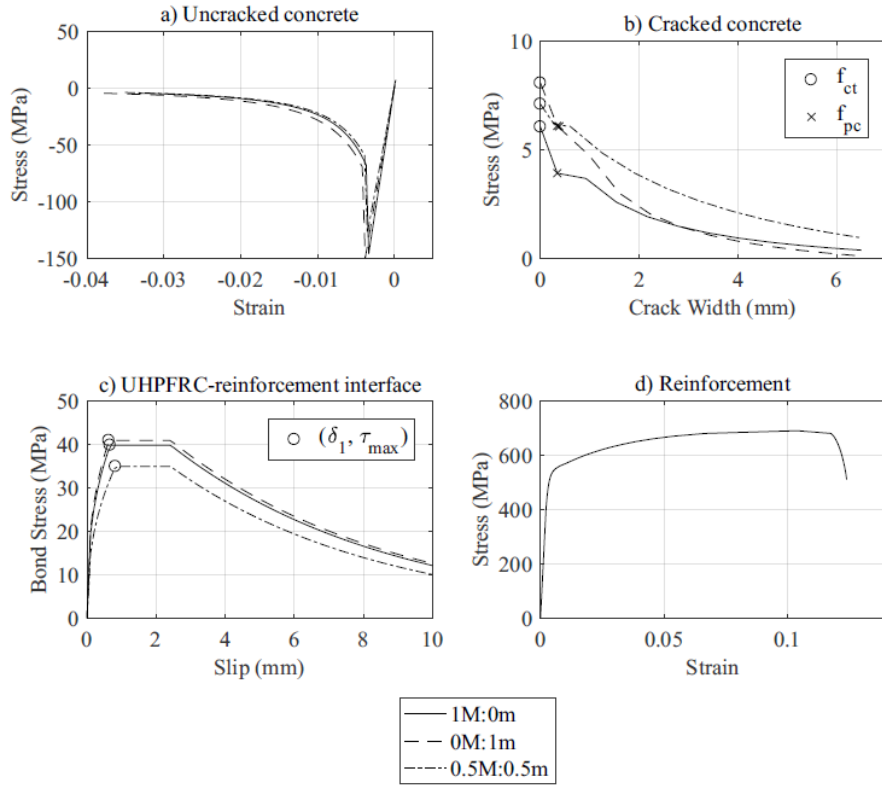


Fig.1 Concrete and reinforcement material properties

All beams were reinforced with deformed steel reinforcing bars complying with AS/NZS 4671:2001 [30]; the stress-strain relationship of the reinforcement is illustrated in Fig. 1(d) and has a yield strength of 535 MPa, and an ultimate strength of 690 MPa at an average strain of 0.104.

3. BEAM TEST SPECIMENS

The two cross-sections in Fig. 2 were chosen so that the effect of stirrups and beam size could be studied. The beam has a tensile reinforcement ratio of 1.2% and the slab 0.57%. Significant cover was allowed around all reinforcement to help facilitate uniform fibre distribution.

The UHPFRC was produced in a pan mixer with a capacity of 500 litres by first mixing the sand, cement, silica fume together for 1 minute. The superplasticiser and water were then added

and the contents mixed until visibly flowable. Finally, the steel fibres were added and mixed for a further 5 minutes. During casting, a stick vibrator was used sparingly to assist compaction. After casting, the beams and all associated material test specimens were allowed to cure for 28 days by wetting and then covered with plastic to prevent evaporation.

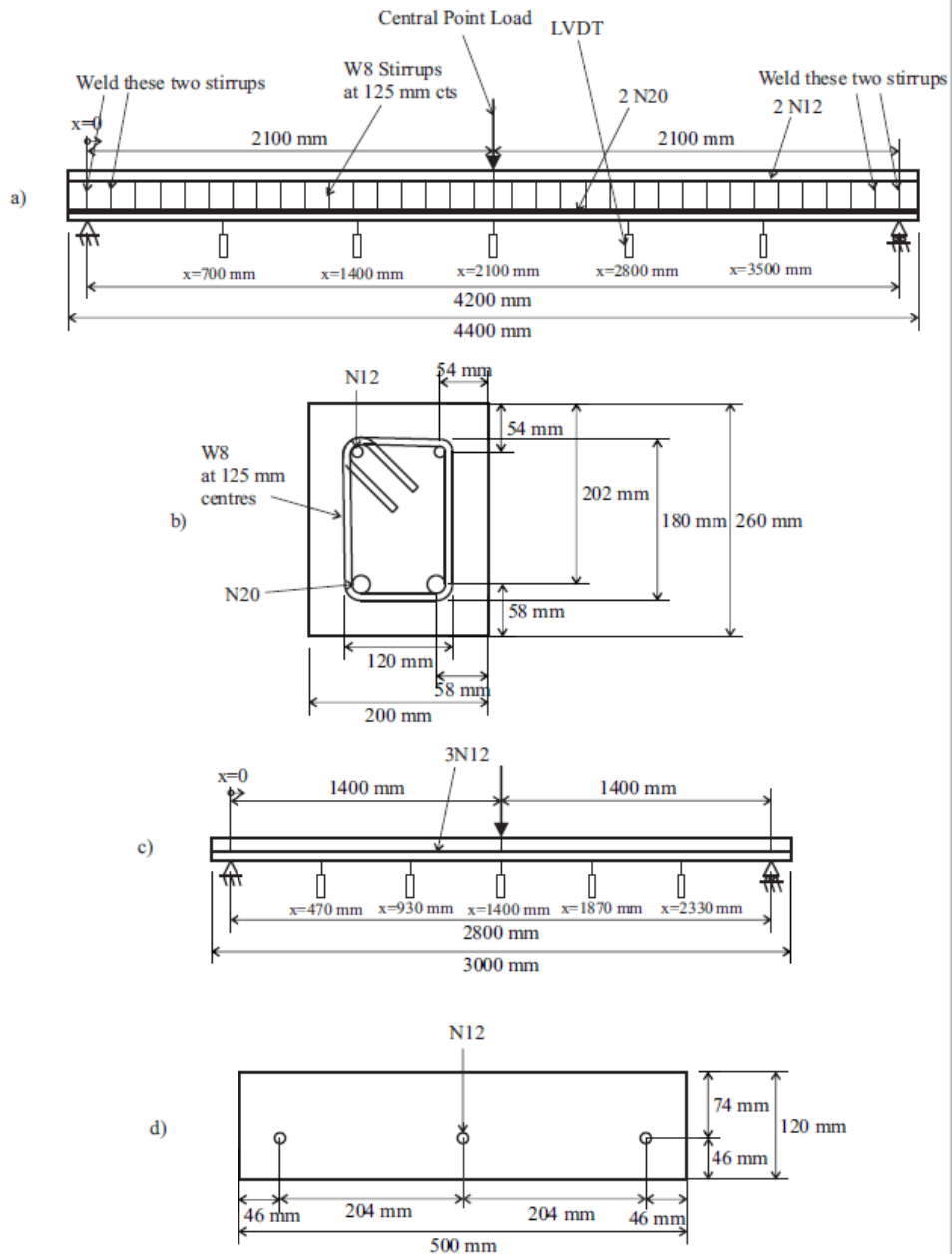


Fig. 2: Test specimens: a) elevation of beam section; b) cross-section of beam section; c) elevation of slab section; d) cross-section of slab section

4. TESTING PROCEDURE

All the members were tested under three point bending at a rate of 2 kN/min for the beams or 1 kN/min for the slabs until the slope of the load-deflection curve changed indicating that the load was close to the peak load. The different load rates were chosen as the expected maximum load for the slab sections was expected to be approximately 50% of that of the beam sections, hence the peak load would after approximately the same test duration. The test was then continued at a displacement rate of 5 mm/min for both sections until: either the tensile reinforcement ruptured in the beam or a deflection of 100 mm was reached in the slab. This 100 mm limit was put in place to protect the instrumentation. The deflections were measured using a string of 5 LVDTs as shown in Fig. 2(a) and 2(c). The crack widths were measured using a handheld optical microscope with a magnification of 220 times at 20, 40 and 60 kN loads for the beams and at 20 and 30kN for the slabs, The crack widths were only measured on the rising branch as crack widths are of interest primarily at serviceability.

5. RESULTS

The mid-span load-deflection responses of all members are given in Fig. 3. Further, a summary of the load and deflections at each load increment at which the crack width was measured as well as at reinforcement yield, commencement of concrete crushing and at reinforcement rupture is given in Table 4.

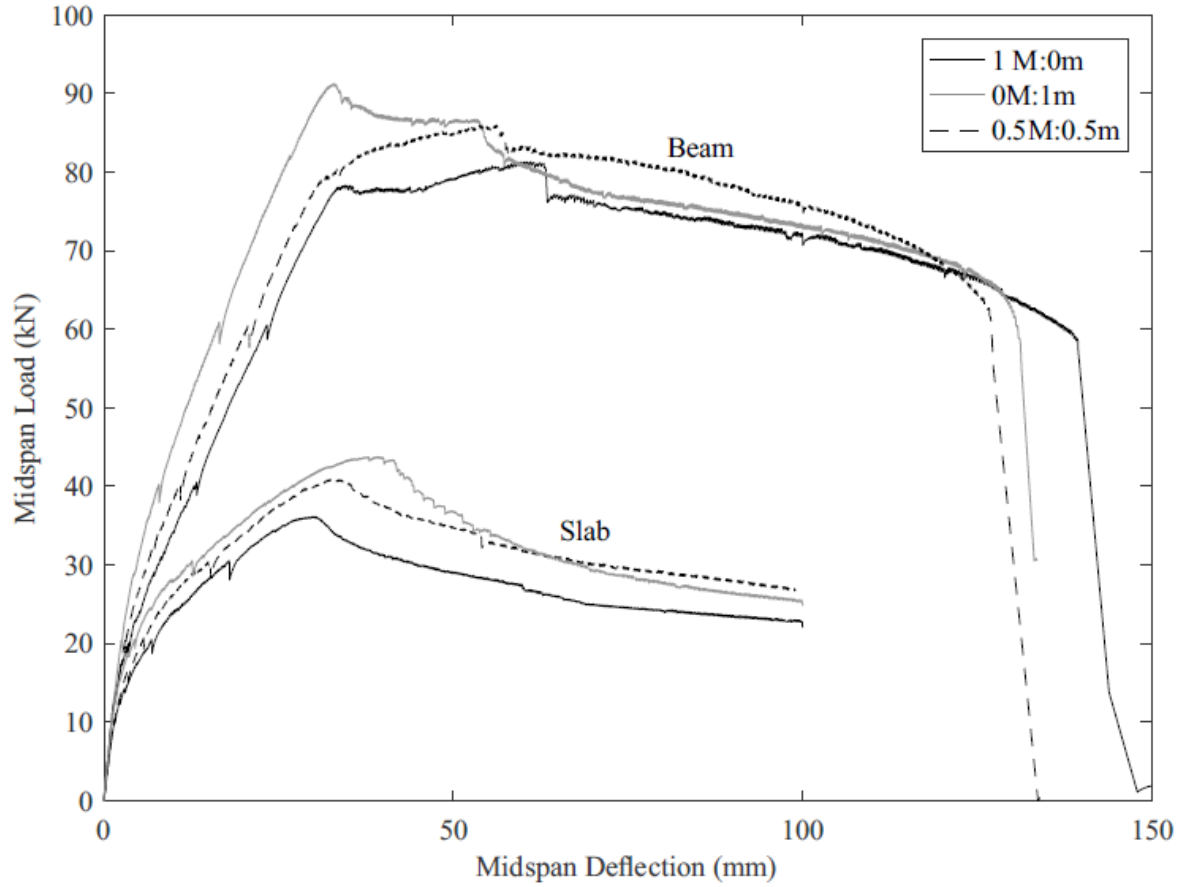


Fig. 3 Mid-span Load-Deflection

Table 4. Mid-span Load and Deflection at Key Points

		1M:0m		0M:1m		0.5M:0.5m	
Section		Δ_{mid} (mm)	P (kN)	Δ_{mid} (mm)	P (kN)	Δ_{mid} (mm)	P (kN)
Beam	P=20 kN	3.73	20.0	2.53	20.0	3.12	20.0
	P=40 kN	13.5	40.0	8.24	40.0	10.7	40.0
	P=60 kN	23.1	60.0	16.9	60.0	21.4	60.0
	Yield	33.7	78.0	32.9	91.2	31.1	78.6
	Crushing	61.1	81.3	53.3	86.3	56.3	86.0
	Rupture	139	57.4	131	55.1	127	55.3
Slab	P=20 kN	6.55	20.0	4.53	20.0	5.38	20.0
	P=30 kN	17.5	30.0	13.2	30.0	15.8	30.0
	Yield	30.1	36.1	39.2	43.8	32.4	40.9
	$\Delta_{mid}=100$ mm	100	22.7	100	24.8	100	26.9

Note: Δ_{mid} is the midspan deflection and P is the applied load

From the load deflection relationships in Fig. 3, it can be seen that replacing micro-fibres with macro-fibres has the following significant effects.

- Reduces the serviceability or ascending branch stiffnesses when the crack widths are small. This is because for a given volume of fibres the macro-fibres have a smaller bonded perimeter than the micro-fibres. Hence their contribution to the axial tensile stiffness will be reduced, at small crack widths, as the stress in a macro-fibre increases more slowly with slip than for micro-fibres [31].
- Reduces the moment at yield. This is again because of the reduced bonded perimeter of fibres.
- Increases the deflection at reinforcement fracture. This is because at large crack widths the macro-fibres can span the cracks whilst micro-fibres tend to pull out. Note however that the load carried by the blended mix (0.5M:0.5m) is the greatest after crushing of the concrete. This is due to the micro-fibres contributing at the narrow crack tip while the macro-fibres contribute at the crack mouth.

A summary of the crack widths measured within the central 1 m span of each beam is provided in Table 5. As expected due to the random distribution of fibres and the semi-random nature of cracking the scatter is large [32]. However, it can still be seen that 1M:0m had larger crack widths for every measurement. The maximum crack widths were similar between 0.5M:0.5m and 0M:1m; this behaviour is to be expected as the inclusion of micro-fibres increases the overall number of fibres crossing a crack, hence increasing the bonded perimeter for the same volume and, therefore, the crack-opening stiffness is increased. The average crack widths were similar between the mixes, however more cracks were observed for the mixes with greater numbers of macro-fibres. The proposed reason for this is that cracks with widths less than 0.05 mm are difficult to identify consistently. Hence, if the average crack widths are smaller for

beams with micro-fibres consistent with the behaviour of the maximum crack width values a greater number of cracks would be undetected reducing the number of cracks observed.

The hinge region at the end of each test is shown in Fig. 4. The beams in Figs. 4(a-c) failed by reinforcement rupture at a large central crack above which minor concrete crushing was observed. In the slabs in Figs. 4(d-f), testing was stopped at a central deflection of 100 mm at which point a large central crack had also occurred but there was negligible crushing of the concrete.

Table 5: Crack Widths

Section	P (kN)	1M:0m			0M:1m			0.5M:0.5m		
		Number of cracks	w_{ave} (mm)	w_{max} (mm)	Number of cracks	w_{ave} (mm)	w_{max} (mm)	Number of cracks	w_{ave} (mm)	w_{max} (mm)
Beam	20	4	0.037	0.047	1	0.016	0.016	2	0.037	0.044
	40	22	0.049	0.162	9	0.027	0.058	23	0.028	0.058
	60	29	0.056	0.166	21	0.047	0.162	31	0.038	0.097
Slab	20	14	0.038	0.119	7	0.026	0.034	10	0.027	0.062
	30	37	0.050	0.329	13	0.060	0.138	20	0.035	0.106

Note: w_{ave} is the average crack width and w_{max} is the maximum crack width

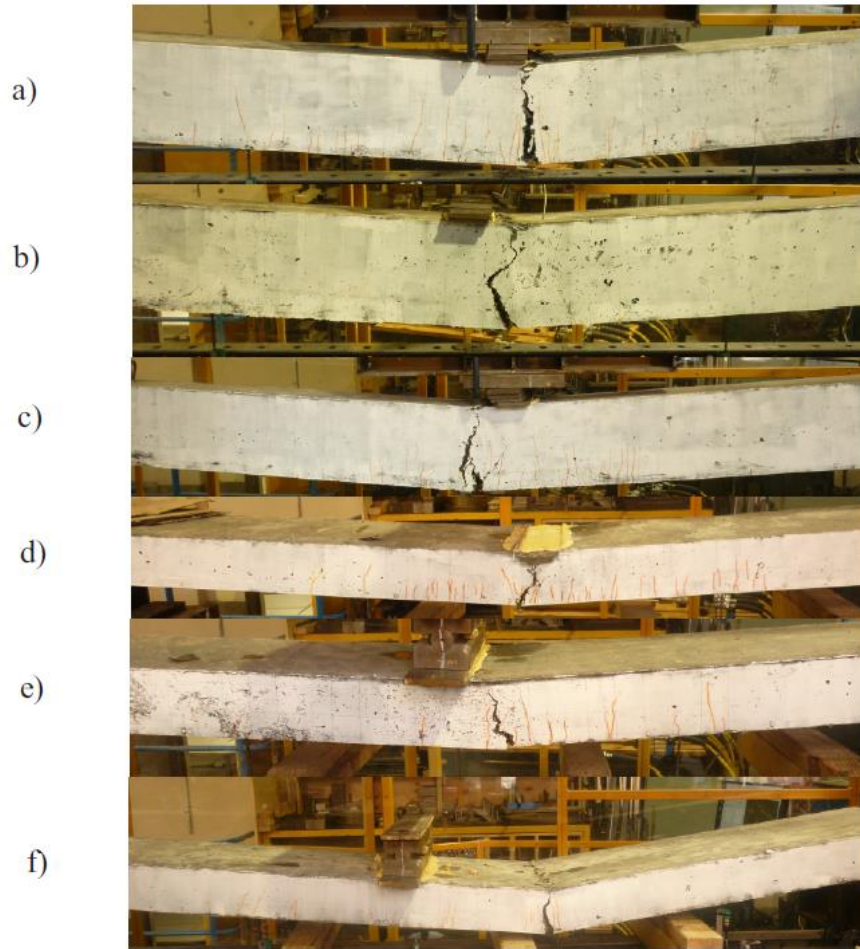


Fig. 4. Hinges at failure: a) 1M:0m (Beam); b) 0M:1m (Beam); c) 0.5M:0.5m (Beam); d) 1M:0m (Slab); e) 0M:1m (Slab); f) 0.5M:0.5m (Slab)

6. SEGMENTAL ANALYSIS

A displacement based segmental analysis approach for fibre reinforced concrete developed by Visintin & Oehlers [23] was used in the following analysis as it requires only the input of basic material properties such as the compressive and tensile stress-strain relationships and the local bond stress-slip relationship. A brief description of the fundamental mechanics of the approach is provided in the following section, but the reader is referred to Visintin & Oehlers [23] for a full treatment. It should also be noted that a range of other displacement based approaches for

the analysis of conventional and fibre reinforced concrete have been developed [1;21-23], with the main difference being in the level of empirical approximation made in simulating the formation and widening of cracks, tension stiffening and concrete softening.

Consider the segment in the uncracked region of the beam in Fig. 5(a) that is significantly shorter than the span of the beam. In order to determine the sectional properties of the beam, let the segment be subjected to a constant moment such that symmetry around the mid-point of the segment now exists. This allows for the consideration of only the half-segment of length L_{def} as shown in Fig. 5(b). The depth of the neutral axis is d_{NA} and the segment end is rotated about this depth by an angle θ such that the deformation profile along the member depth $D(y)$ is defined.

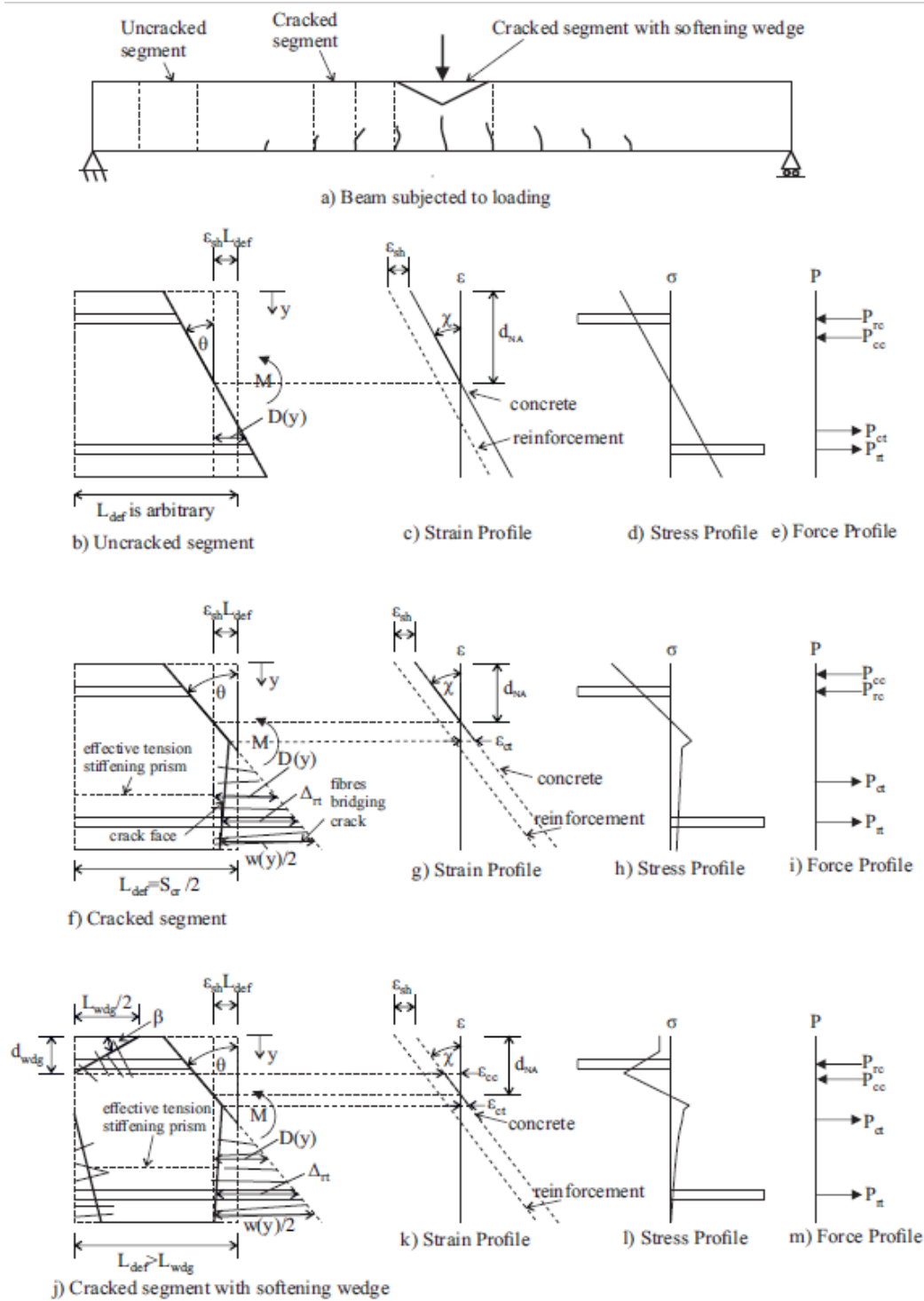


Fig. 5 Segmental Analysis

The strain profile in Fig. 5(c) is simply $D(y)/L_{def}$ and as the segment has been extracted from an uncracked region, the stiffnesses of the reinforcement and concrete in Fig. 1 can now be used to derive the stress profile in Fig. 5(d). From the stress profile the forces in Fig. 5(e) can

be derived, and it is then a matter of adjusting d_{NA} in Fig. 5(b) until longitudinal equilibrium is obtained. This analysis gives the relationship between the segment end rotation θ and the applied moment M . Further, because the curvature χ is θ/L_{def} , the relationship between the curvature and moment, that is, the sectional property, up until a crack forms can also be determined. It is important to note here that because no strain localisations exist, the analysis technique is identical to a standard moment curvature approach and yields identical M/χ relationship regardless of the segment length, hence the segment length at this stage is arbitrary as indicated in Fig. 5(b).

Now consider the cracked segment in Fig. 5(a) of total length equal to the crack spacing S_{cr} such that the deformation length for analysis is $S_{cr}/2$ as in Fig. 5(f). The widening of the crack Δ_{rt} is known to be the result of a build-up of stresses in the tension region through the bond-slip between the reinforcement and the surrounding concrete and will be used directly to determine the force in the tensile reinforcement P_{rt} as described in the following section.

For analysis of the beam segment in Fig. 5(f), a rotation is again applied to the segment end to give the segment deformation $D(y)$. For the compression region and the uncracked tension region, the strain profile in Fig. 5(g) can be determined as for the uncracked region Fig. 5(b) that is material constitutive relationships can be applied to determine the resulting stresses and forces in Figs. 5(h) and (i) respectively. For the cracked concrete in tension in Fig. 5(f), the stress in the concrete can be determined from the deformation profile using the material stress-crack width relationship shown in Fig. 1(b) given a relationship exists between the segment deformation, $D(y)$ and the crack width, $w(y)$. The deformation is given by the addition of the crack opening and the material deformation of the uncracked concrete away from the crack [33]. That is

$$D(y) = \varepsilon(y)L_{def} = \frac{w(y)}{2} \frac{L_{def}}{\left(\frac{S_{cr}}{2}\right)} + \frac{\sigma_c[w(y)]}{E_c} L_{def} \quad (1)$$

where the first term on the right hand side is the deformation due to crack opening, in which $L_{def}/(S_{cr}/2)$ represents the number of half crack widths in the segment (this allows for concrete crushing where the segment length can extend over multiple crack spacings), and the second term represents the deformation due to the stress in the concrete, $\sigma_c(w)$, which is a function of the crack width and E_c is the elastic modulus of the concrete. In terms of the effective strain Eq. (1) yields

$$\varepsilon(y) = \frac{w(y)}{S_{cr}} + \frac{\sigma_c[w(y)]}{E_c} \quad (2)$$

which can be used to construct a relationship between the effective strain and the crack width by substituting the crack width and corresponding stress for each point in Fig. 1(b) and evaluating the resultant effective strain, $\varepsilon(y)$.

For the reinforcement crossing the crack in Fig. 5(f), the force resisted P_{rt} is a function of the slip of the reinforcement from the crack face Δ_{rt} which can be determined through the application of established partial interaction mechanics (e.g. see Gupta & Maestrini [34]; Wu et al. [35]; Balazs [36]; Choi & Cheung [37] Sturm et al. [38]) as outlined in the following section. Having now defined all the internal forces in Fig. 5(i), it is again simply a matter of adjusting d_{NA} until force equilibrium is achieved, after which the moment resisted for a given end rotation θ and consequently curvature can be determined. Similarly, the relationship between the moment and the crack width can be determined by evaluating the effective strain at the depth the crack width is to be evaluated, and then using the relationship defined using by Eq. (2) to find the corresponding crack width.

6.1 Partial interaction mechanics to determine crack spacing, S_{cr} and $P_{rt}-\Delta_{rt}$ behaviour

To determine the crack spacing S_{cr} and the relationship $P_{rt}-A_{rt}$, consider the tension stiffening prism identified in Fig. 5(f) and with cross-section shown in Fig. 6(a), with the elevation of the tension stiffening prism adjacent to uncracked concrete illustrated in Fig. 6(b) and the elevation of a prism between two adjacent cracks is illustrated in Fig. 6(c). The slip of the reinforcement relative to the concrete in Figs. 6(d) is governed by the slip strain

$$\frac{d\delta}{dx} = \varepsilon_r(x) - \varepsilon_c(x) + \varepsilon_{sh} \quad (3)$$

where $\varepsilon_r(x)$ is the strain in the reinforcement in Figs.6(e), $\varepsilon_c(x)$ is the strain in the concrete in Fig. 6(f) and ε_{sh} is the shrinkage strain. Considering the equilibrium of a single infinitesimal element of length dx extracted from Fig. 6(b-c) and shown in Fig. 6(g), it can be shown that the change in stress across the element is given by

$$\frac{d\sigma_r}{dx} = \frac{\tau(x)L_{per}}{A_{rt}} \quad (4)$$

$$\frac{d\sigma_c}{dx} = -\frac{\tau(x)L_{per}}{A_{ct}} \quad (5)$$

in which L_{per} is the total perimeter length of the reinforcement within the tension stiffening prism, A_{rt} is the total area of reinforcement and A_{ct} is the total area of concrete. In order to ensure that no variation in strain is imposed on the tension stiffening prism, the total height of the prism is taken as twice the cover to the centre of the reinforcement and the width is taken as that of the cross section, as shown in Fig. 6(a).

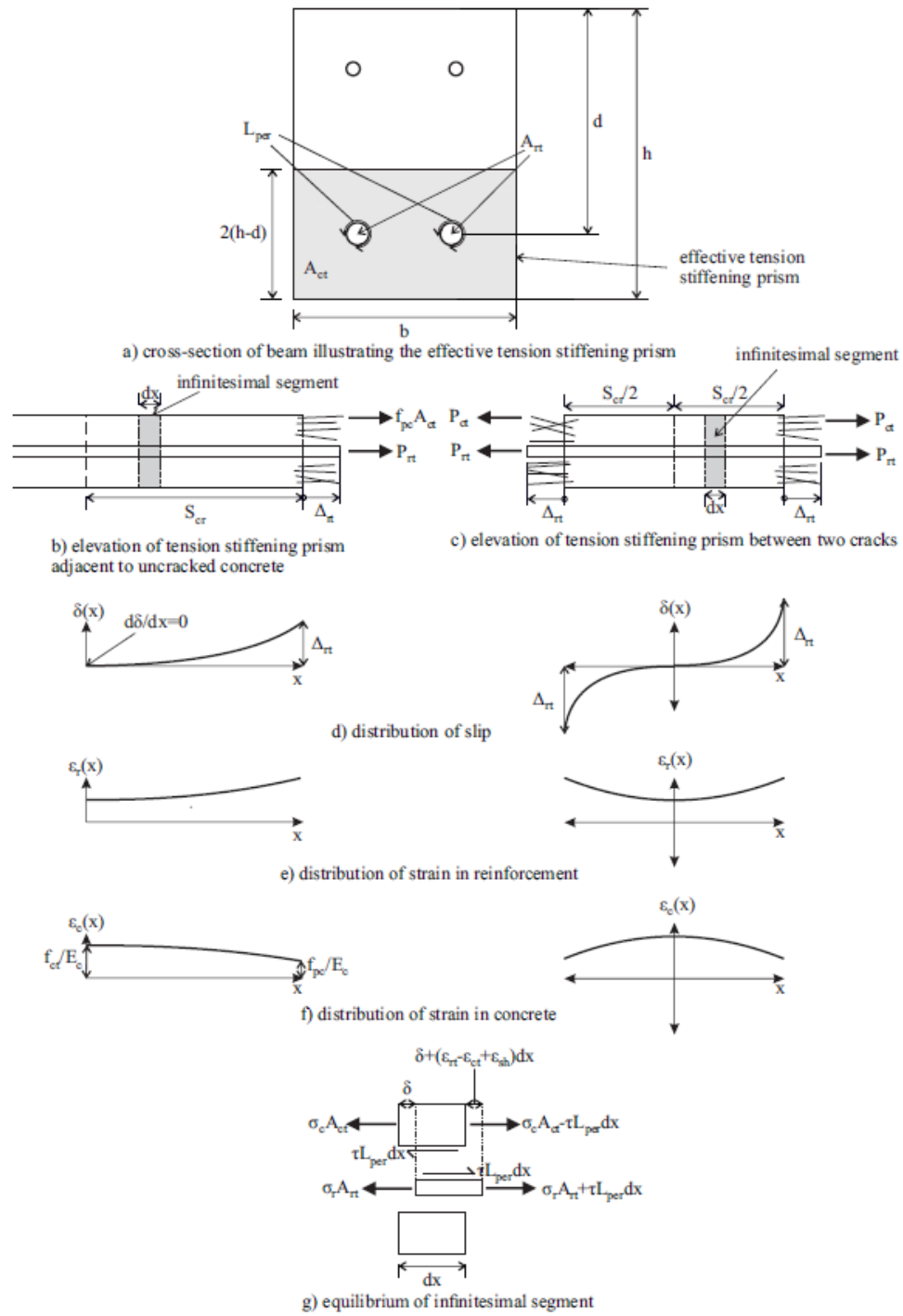


Fig. 6: Analysis of tension chord

For analysis, the three first order differential equations in Eqs. (3-5) can be solved using the initial values for these parameters at the crack face as well as an additional boundary condition depending on the loading scenario. That is to determine the crack spacing S_{cr} , the ‘segment

adjacent to uncracked region' and extending into the uncracked region in Fig. 6(b) is considered along with the boundary condition that the slip and the slip strain equal zero at the same location and the stress in the concrete is also equal to the tensile strength, f_{ct} at the position of the new crack. Sturm et al. [38] solved this problem analytically to yield the following closed form solution for the crack spacing

$$S_{cr} = \left[\frac{2^\alpha(1+\alpha)}{\lambda(1-\alpha)^{1+\alpha}} \right]^{\frac{1}{1+\alpha}} \left[\frac{f_{ct}-f_{pc}}{E_c} \left(\frac{E_c A_{ct}}{E_r A_{rt}} + 1 \right) \right]^{\frac{1-\alpha}{1+\alpha}} \quad (6)$$

where

$$\lambda = \frac{\tau_{max} L_{per}}{\delta_1^\alpha} \left(\frac{1}{E_c A_{ct}} + \frac{1}{E_r A_{rt}} \right) \quad (7)$$

and τ_{max} is the maximum bond stress, δ_1 is the slip at the maximum bond stress and α is the non-linearity of the bond stress-slip relationship, f_{pc} is the post-cracking strength, E_c is the elastic modulus of the concrete and E_r is the elastic modulus of the reinforcement. In Fig. 7(a) τ_{max} , δ_1 and α are defined in terms of the diagrammatic bond stress-slip relationship and in Fig. 7(b) f_{ct} and f_{pc} are defined in terms of the tensile stress-crack width relationship that is also shown in Fig. 1(b).

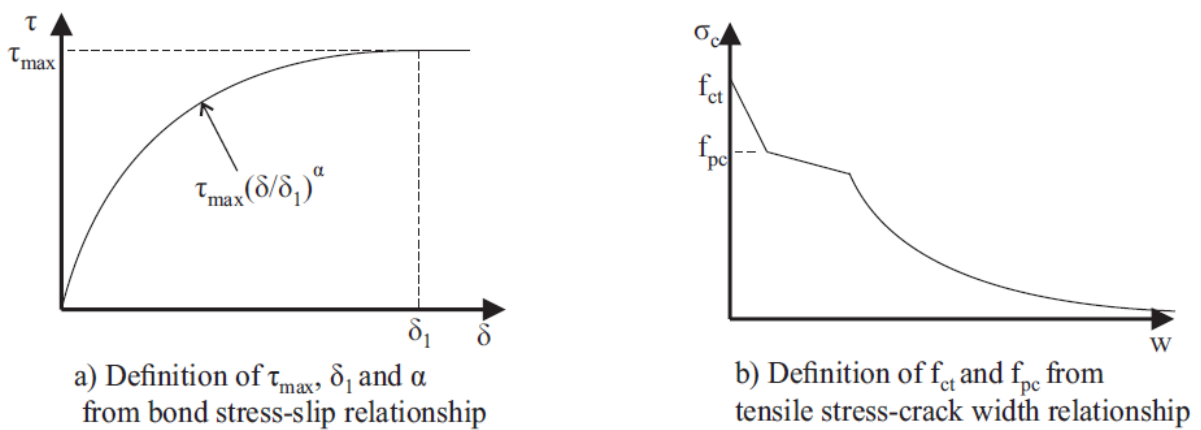


Fig. 7 Definition of parameters in crack spacing expression

To determine the $P_{rt}-\Delta_{rt}$ relationship, the ‘segment between cracks’ is considered with the boundary condition that at the mid-point between two cracks the slip is zero, as shown in Fig. 6(c). This procedure to evaluate this relationship is summarised in the flow chart shown in Fig. 8.

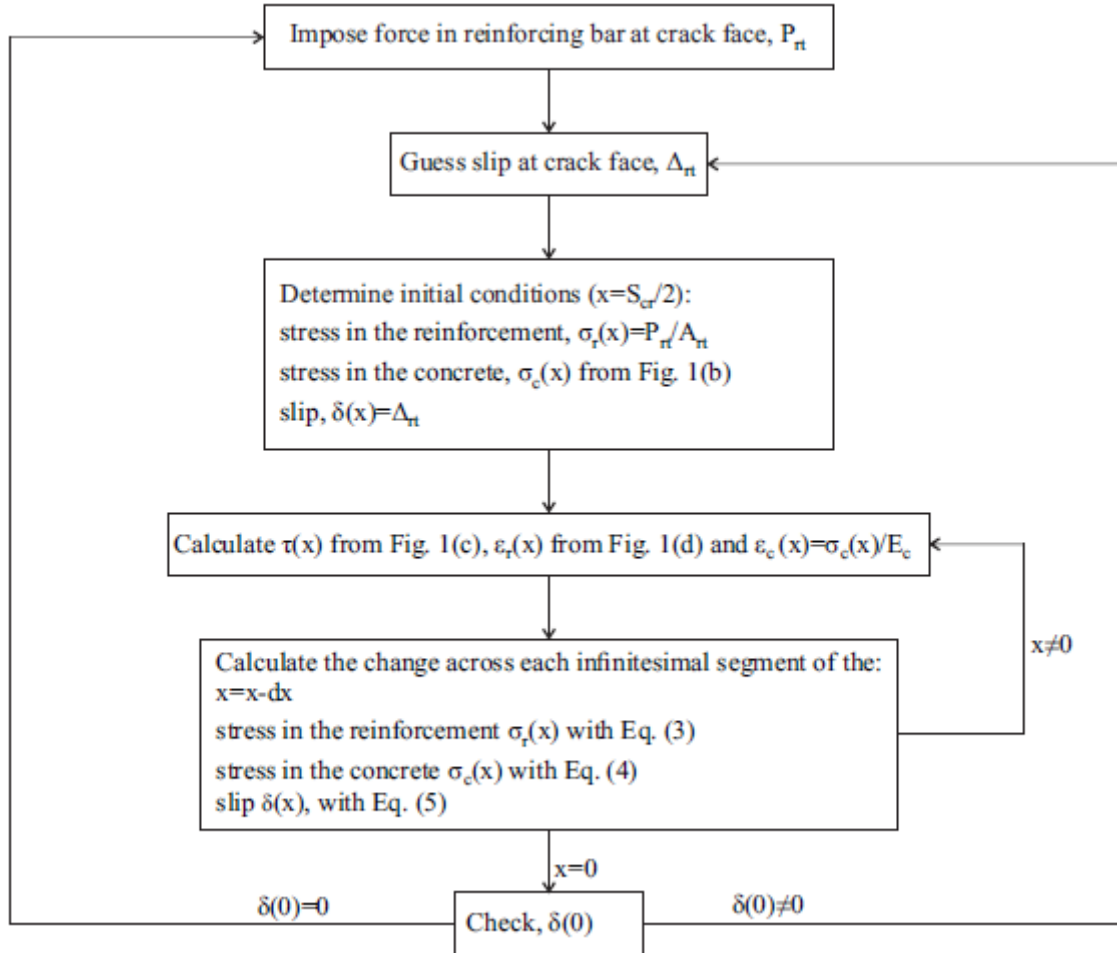


Fig.8: Tension chord analysis procedure

6.2 Accommodation of concrete softening

Finally, in order to allow for the formation and sliding of concrete softening wedges in Fig. 5(a), the length of the segment L_{def} is extended to cover sufficient crack spacings such that the wedge length L_{wdg} is encompassed as in Fig. 5(j).

From Fig. 5(j), the depth of the softening wedge is

$$d_{wdg} = d_{NA} + \frac{\varepsilon_{cc}}{\chi} \quad (8)$$

in which ε_{cc} is the strain corresponding to the peak compressive strength f_c .

Based on the depth of the wedge, its length can be determined geometrically as the angle at which it is formed β is known. That is

$$L_{wdg} = \frac{2d_{wdg}}{\tan \beta} \quad (9)$$

in which according to Mohamed Ali et al. [39]

$$\beta = \arctan(-m + \sqrt{m^2 + 1}) \quad (10)$$

where m is the slope of the curve relating the shear capacity to the normal stress on the sliding plane. From shear friction tests conducted by Sturm et al. [26] for the same UHPFRC mix design, β is 14° .

Having defined the length of the softening region and consequently L_{def} required for analysis when the concrete is softening, the stress-strain relationship obtained from a standard material prism of height L_{test} can be made size dependent to allow for the change in ductility associated with the length of the softening region L_{def} [1,21]. This size dependent conversion is achieved here using the approach of Chen et al. [40] as follows given by

$$\varepsilon_c = \sigma_c/E_c + (\varepsilon_{test} - \sigma_c/E_c) \frac{L_{test}}{L_{def}} \quad (11)$$

in which, ε_{test} is the experimental measured strain and σ_c/E_c is the material strain. The size dependent stress strain relationship is now used in Figs. 5(j)-(m) to simulate the ductility of the softening region. The procedure is identical to that for the cracked segment in Figs. 5(f)-(i) described above.

A flow chart outlining the entire analytical procedure described in this section is shown in Fig.

9.

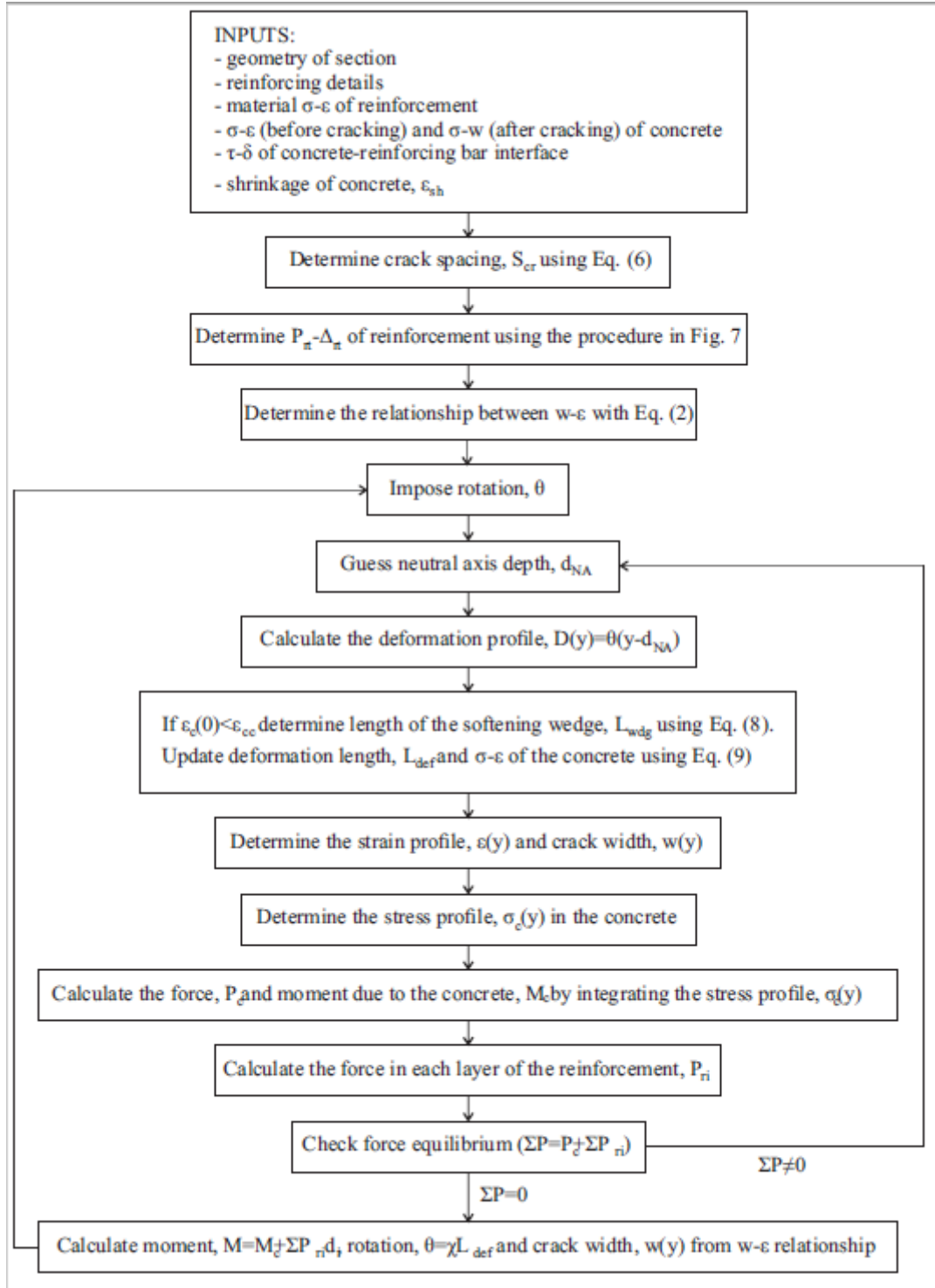


Fig. 9 Procedure for generating moment-rotation, moment-curvature and moment-crack width relationship

7. VALIDATION

The segmental analysis was used to simulate the tested beams using the material properties in Fig. 1 and Table 1. The load-deflections are compared in Figs. 10 where it can be seen that there is a close correlation. The predicted load-deflections were terminated when the tensile strength of the reinforcement was reached because the length over which necking occurs cannot be predicted. There is a good correlation between the predicted and actual maximum crack widths in Fig. 11 for the slab sections, however for the beam sections, it was found that predictions tended to overestimate the maximum crack width, although, they were closer at lower loads. One cause of this discrepancy is the tendency for secondary cracks to form in between the primary cracks which would decrease crack widths. Scatter of crack widths can also be expected to occur due to the random distribution of fibres within the member.

In Fig. 10 the results from the segmental analysis are also compared to results obtained using a conventional sectional analysis. The assumptions include plane section remain plane and the strain in the bonded reinforcement is the same as the surrounding concrete. The effect of tension stiffening on the stress response of the reinforcement is neglected and the stress-crack width relationship of the tensile concrete is converted into a stress-strain relationship by dividing by a characteristic length. This is assumed to be $\frac{2}{3}$ the total depth of the section [41]. A hinge length was also required to determine the deflection corresponding to the softening portions of the moment-curvature relationship. There is no guidance on this value in AFGC [41] so this was taken as 1.2 times the full depth of the section as this is the value used to assess plastic rotations in the Eurocode 2 [42]. From this comparison it can be seen that similar results are obtained on the ascending branch. This is the case as the magnitude of the tension stiffening is small for UHPFRC sections as the post-cracking stress at the crack is close to the tensile strength. The sectional analysis also provided an accurate estimate of the peak loads, however,

it could not predict the deflection after yield. Hence the conventional sectional analysis cannot be used to assess the ductility of these sections. As the ductility is important to assessing the performance of these sections the segmental analysis was adopted for the parametric study.

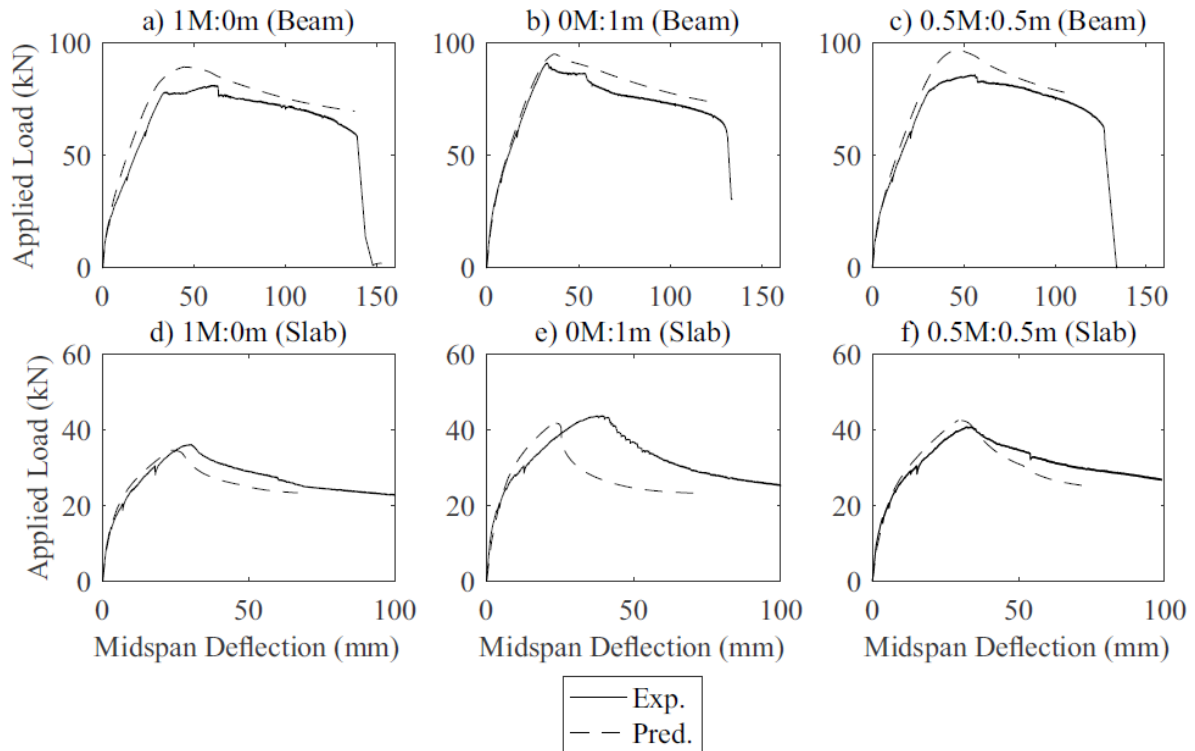


Fig. 10 Predicted to Experimental Load-Deflection

In Fig. 11 the predicted maximum crack widths are also compared between the expression from AFGC [41] and the segmental analysis. From this comparison it is seen that the segmental analysis provides a more accurate assessment of the maximum crack width than the codified expression.

Of particular importance for the analysis of UHPFRC is the consideration of tension stiffening behaviour post-yield and prior to necking as it was found that bond has a significant impact on the overall strain prior to reinforcement rupture and, therefore, in the prediction of the ductility of the beams. Yielding of the tensile reinforcement results in a reduction of bond stress due to

the lateral contraction of the bar. This has been observed experimentally for conventional reinforced concrete structures and many expressions for the reduction of bond after yielding have been suggested [43-51]. No research has however been completed to date on whether this reduction in post-yield behaviour differs for UHPFRC. As no further information was available the expression suggested by Malek et al. [51] was adopted where the bond stress after yield is given by

$$\tau(\varepsilon_r) = \tau_{max} \left(1 - A \left\{ 1 - \exp \left[B \left(1 - \frac{\varepsilon_r}{\varepsilon_y} \right) \right] \right\} \right) \quad (12)$$

where $A=0.8$ and $B=0.7$ and ε_y is the yield strain. This expression was found to give a close fit for the beam sections, however, for the slab sections the ultimate deflection was underestimated. A better fit was obtained for the slabs when a value of $A=1$ was used implying that the bond after yielding was lower. The most likely explanation for this discrepancy is the presence of stirrups in the beam section which matches the situation in the tests conducted by Malek et al. [51]. The stirrups allow the transfer of stress between the reinforcement and concrete even when the interface is heavily damaged, hence the bond stress that can be maintained is increased.

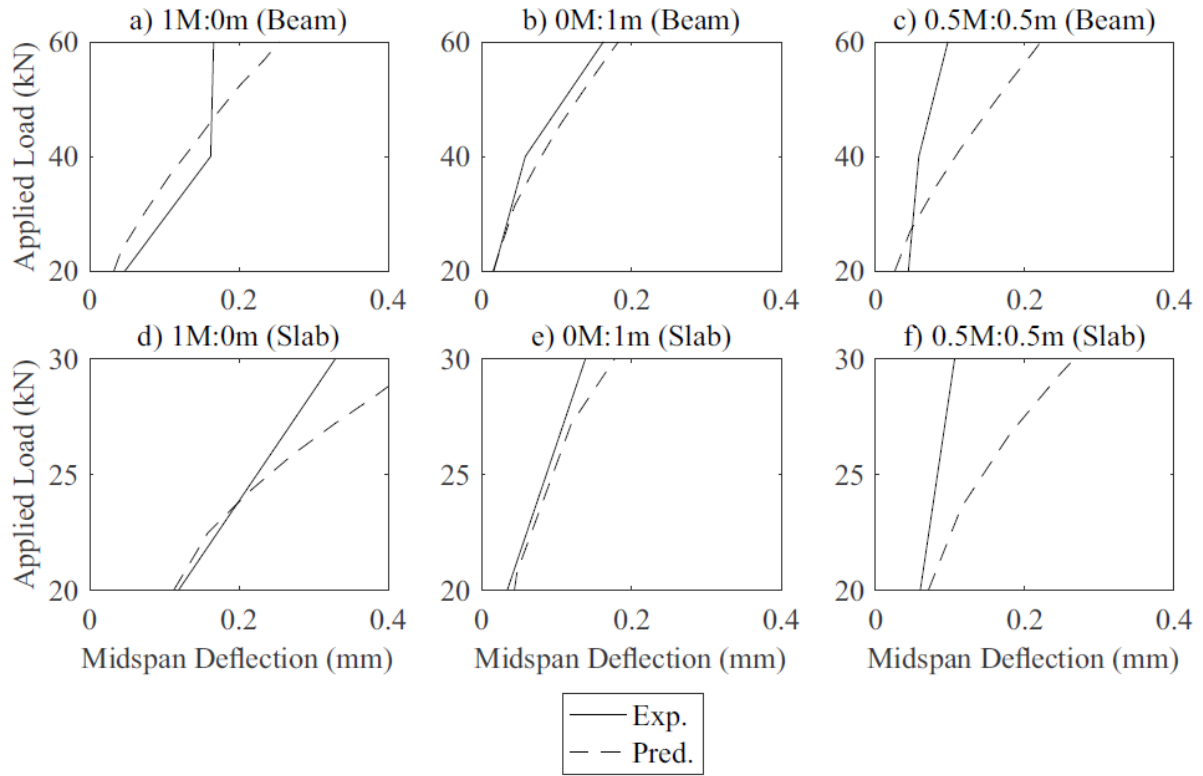


Fig. 11 Predicted to Experimental Load-Crack Width

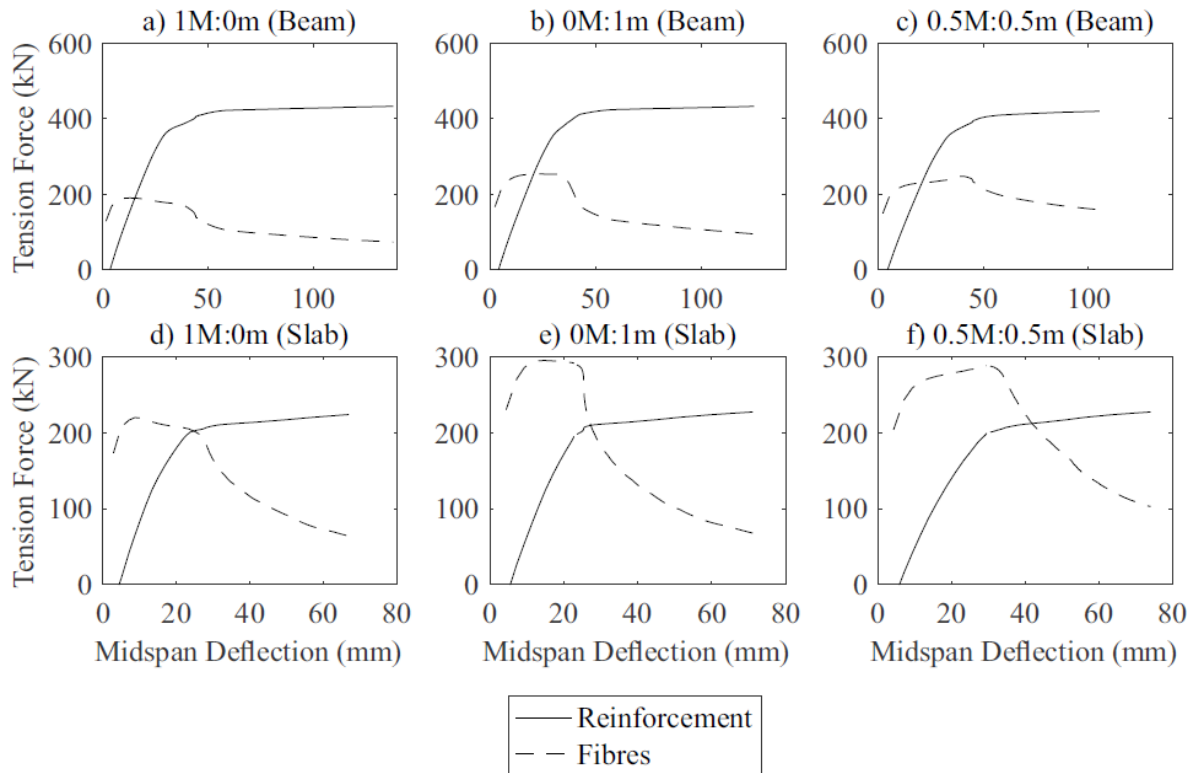


Fig. 12 Relative contribution of reinforcement and fibres

Based on the application of the segmental analysis procedure the relative contributions of the fibres and the tensile reinforcement to the tension forces carried by the beams can be determined as shown in Fig. 12. From this it can be seen that the contribution of fibres is greatest before the yielding of the reinforcement and then decreases post yield. This reduction in force carried by the fibres is due to the rapid increase in crack width that occurs at yielding due to the significant rotation that localises at the crack at the centre of the beam (see Fig. 4). It was also found that the contribution of the fibres was greater for the more lightly reinforced slab sections than it was for the more heavily reinforced beam sections. The contribution of the fibres was also greater for mixes containing micro-fibres (0.5M:0.5m and 0M:1m).

8. PARAMETRIC STUDY

Having validated the analysis approach in the previous section it is now used to perform a parametric study investigating the effect of varying the depth and reinforcement ratio and whether this modifies the conclusions of the experimental study. In Figs. 13 and 14 the load-deflection and load-crack width relationships are illustrated for the cases where the effective depth, d was varied from 202 to 808 mm and the reinforcement ratio, p was varied from 1.00% to 3.05%. The span to depth ratio and the ratio of the compressive to tensile reinforcement was kept constant. From this it was found that varying the depth or the reinforcement ratio did not change the conclusions about the effect of fibre type ascertained from the experimental tests.

As a comparison the segmental approach was also used to simulate a beam without fibres as shown in Figs. 12 and 13. This was performed by assuming that the tensile stress was zero after cracking and the compressive stress was zero after crushing. The concrete strength was assumed to be 160 MPa, the elastic modulus was 48 GPa and the tensile strength was 5.39 MPa

as given by Visintin et al. [16]. The efficacy of the fibres in increasing the strength and stiffness of the sections was observed.

From Fig. 13 it was found that increasing the depth of the section reduced the member ductility due to the size-dependence of the compressive stress-strain relationship [52] while the strength and stiffness of the section increased. In Fig. 15 the relative contributions of the reinforcement and fibres are shown, where it is seen that the percentage contribution of the fibres and reinforcement does not change with depth. The endpoint of the curves in Fig. 15 are achieved when significant crushing has occurred in the compressive concrete and the lack of sensitivity is likely due to the minor impact of fibre blending on the post-softening compressive stress strain behaviour in Fig 1(a).

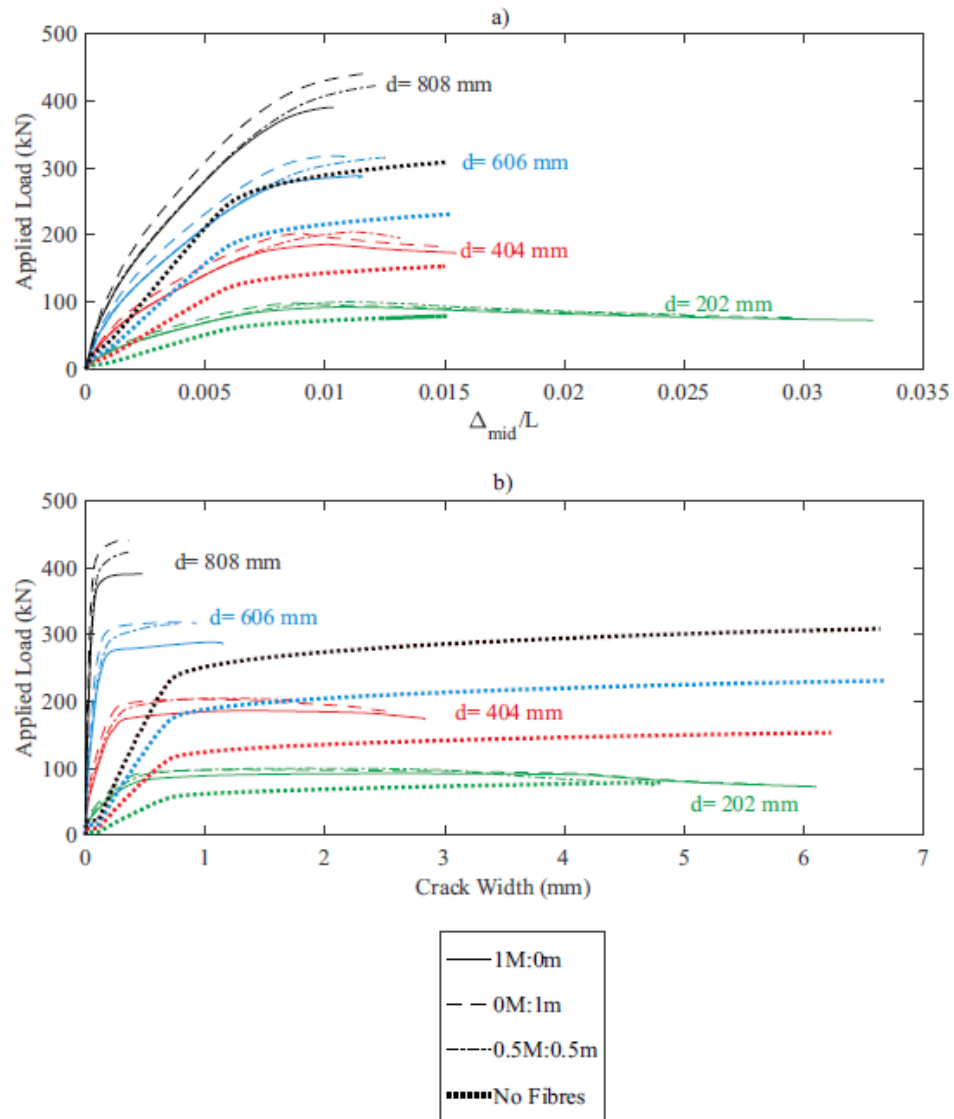


Fig. 13 Effect of depth: (a) load-deflection; (b) load-crack width

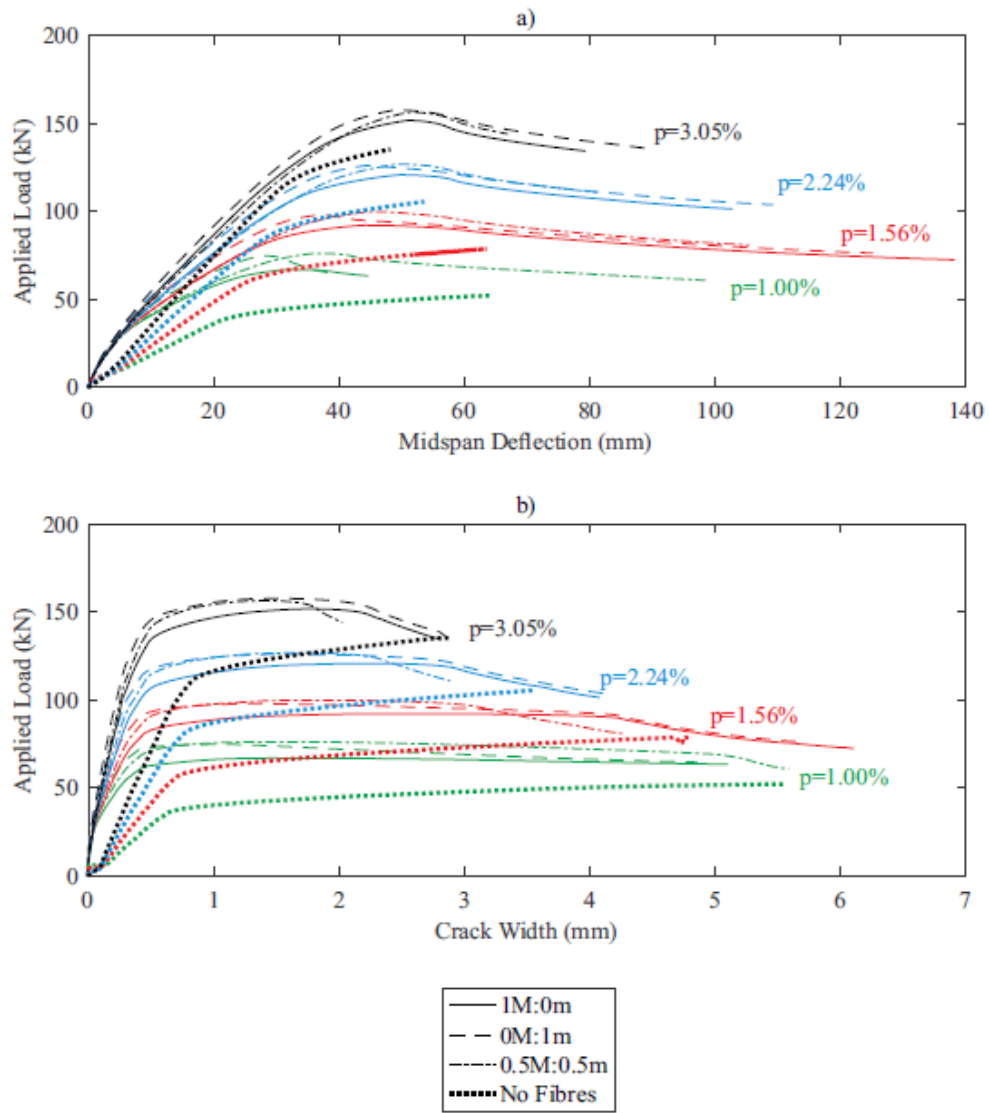


Fig. 14 Effect of reinforcement ratio: (a) load-deflection; (b) load-crack width

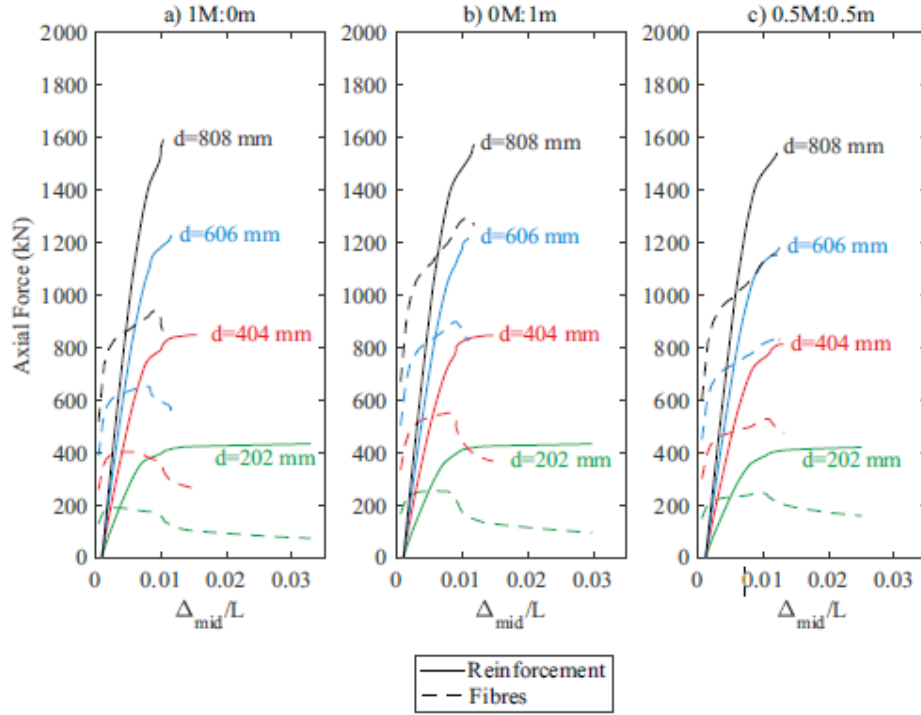


Fig. 15 Relative contribution of reinforcement and fibres when depth is varied

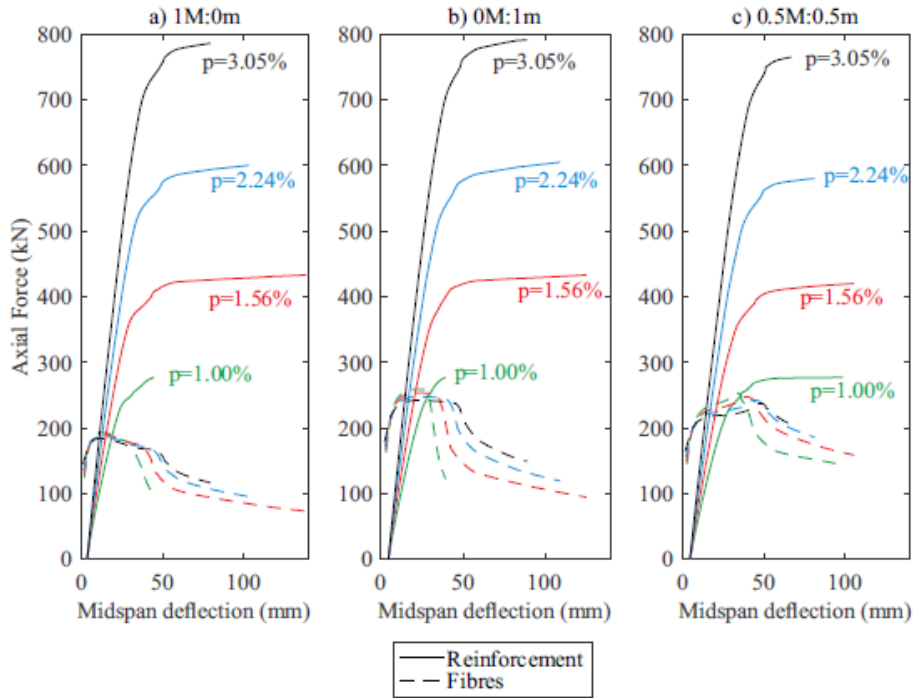


Fig. 16 Relative contribution of reinforcement and fibres where the reinforcement ratio is varied

From Fig. 14 it was found that increasing the reinforcement ratio increases the ductility of members that failed by the rupture of the tensile reinforcement, and reduced the ductility decreases of members that failed by compressive concrete crushing. The strength and stiffness increased with increasing quantities of reinforcement.

For sections with low reinforcement ratios, failure is controlled by the rupture of the tensile reinforcement which is a function of the crack width. In this case an increase in reinforcement ratio results in an increase in ductility. This is the case because an increase in reinforcement ratio results in an increase in the neutral axis depth. The result of this is a higher rotation is required in the segment to achieve the same crack width.

However, for sections with higher reinforcement ratios, failure is controlled by concrete crushing which is a function of the strain in the top fibre. As the neutral axis depth increases the curvature required to achieve a given strain at the top fibre decreases, hence a loss in ductility. The different fibre types have limited effect on the neutral axis depth and the crack to cause rupture tensile reinforcement, hence the different types of fibre did not exert significant influence on the ductility in this case.

In Fig. 16 the relative contributions of the fibres and reinforcement are also explored. It is seen that the force carried by the fibres changes negligibly with changes in the reinforcement ratio and a greater proportion of the load is carried by the reinforcement with increasing reinforcement ratio.

Note that the trends explored in this parametric study are open to further experimental confirmation as the analysis approach used to generate the parametric study was validated on

a relatively small dataset. This maybe significant because of the randomness induced by the fibres will influence member level behaviour.

9. CONCLUSION

Although the benefits of blending fibres of different sizes has been well established at a material level, to date negligible research has considered performance at a structural level. In order to investigate the influence of blending hooked end macro-fibres and straight micro-fibres in UHPFRC a series of six tests were undertaken on slab and beam sections. The results of the experimental work show that members constructed from mixes with only microfibres performed better in terms of increased ultimate strength and reduced deflections and crack widths at serviceability. The substitution of 50% macro-fibres was however found to increase the load that could carried past concrete crushing, although this also reduced the deflection at rupture. In addition to altering mechanical performance, substituting some of the micro-fibres with macro-fibres maybe a valid choice if they improve the economics or reduce the environmental impact of the structure [53].

The results obtained from beam tests were simulated using both standard codified approaches and a numerical segmental analysis technique capable of predicting both member deflection and crack width. From this comparison it was shown that while both approaches could adequately predict member deflection in the serviceability range, the segmental approach could more accurately predict serviceability crack widths as well as member ductility and ultimate deformation.

While the segmental approach was shown to be able to simulate behaviour based only on basic material test results (material shrinkage, uniaxial compression, uniaxial tension, bar pullout

and direct tension of the reinforcement) some uncertainty still exists regarding the influence of reinforcement yield on local bond properties. This was found to be particularly important for UHPFRC beams because they are more susceptible to failure by reinforcement rupture rather than concrete crushing. This suggests further research is required to develop a material model for the post-yield bond behaviour of UHPFRC which reflects all the relevant parameters.

Finally a parametric study, was performed to investigate the effect of depth and reinforcement ratio on the behaviour of UHPFRC beams with blended fibres. Varying the depth or the reinforcement ratio did not affect the conclusions regarding the effect of blending fibres. However, a large size effect was predicted on the ductility of UHPFRC beams which should be experimentally verified.

ACKNOWLEDGEMENTS

This material is based upon work supported by the Air Force Office of Scientific Research under award number FA2386-16-1-4098 and Australian Research Council Discovery Project DP190102650. The authors also acknowledge the assistance of Mr Nicholas Burton in measuring the crack widths during the experimental program.

NOTATION

A, B = parameters in post-yield bond stress-reinforcement strain relationship;

A_{ct} = area of tension chord;

A_{rt} = cross-sectional area of reinforcement;

b = width of section;

D = deformation;

d_{NA} = neutral axis depth;

d = effective depth;

d_i = depth of the i^{th} layer of reinforcement;

d_{wdg} = depth of softening wedge;

$d\delta/dx$ = slip strain;

E_c, E_r = elastic modulus of concrete and reinforcement, respectively;

f_c = compressive strength;

f_{ct} = tensile strength;

f_{pc} = post-cracking strength;

h = height of section;

L = span;

L_{def} = deformable length;

L_{per} = bonded perimeter of reinforcement in tension chord;

L_{test} = length of test specimen;

L_{wdg} = length of softening wedge;

M = applied moment;

m = slope of shear strength-normal stress relationship;

M_c = moment in the concrete and the reinforcement, respectively;

P = applied load;

P_c = axial force in the concrete;

P_{cc} = axial force in the compressive concrete;

P_{ct} = axial force in the tensile concrete;

P_{ri} = axial force in the i^{th} layer of reinforcement;

P_{rc} = axial force in the compressive reinforcement;

P_{rt} = axial force in the tensile reinforcement;

p = reinforcement ratio;

S_{cr} = crack spacing;

V_f = fibre volume

w = crack width;

w_{ave} = average crack width;

w_{max} = maximum crack width;

x = horizontal position

y = depth (with respect to the top fibre);

α = exponent of bond-slip relationship;

β = angle of softening wedge;

Δ_{mid} = midspan deflection;

Δ_{rt} = slip of the reinforcement at crack face;

δ = slip;

δ_1 = slip at maximum bond stress;

ε = effective strain;

$\varepsilon_c, \varepsilon_r$ = strain in the concrete and the reinforcement, respectively;

ε_{cc} = strain to cause crushing;

ε_{ct} = strain to cause cracking;

ε_{sh} = shrinkage strain;

ε_{test} = strain measured during compression test;

ε_y = yield strain of the reinforcement;

θ = rotation;

λ = bond parameter;

σ_c, σ_r = stress in concrete and reinforcement, respectively;

τ = bond stress;

τ_{max} = maximum bond stress;

χ = curvature;

REFERENCES

1. Schumacher P. Rotation capacity of self-compacting steel fiber reinforced concrete. Ph.D. Thesis, Delft University of Technology, Netherlands, 2006
2. Di Prisco M, Plizzari G, Vandewalle L. Fibre reinforced concrete: new design perspectives. *Materials and structures*, 2009; 42(9): 1261-1281.
3. Oh BH. Flexural analysis of reinforced concrete beams containing steel fibers.” *J. Struct. Eng.* 1992;118(10): 2821-2835.
4. Katzer J, Domski J. Quality and mechanical properties of engineered steel fibres used as reinforcement for concrete. *Construction and Building Materials* 2012; 34: 243-248.
5. Sun W, Chen H, Luo X, Qian H. The effect of hybrid fibers and expansive agent on the shrinkage and permeability of high-performance concrete. *Cement and Concrete Research* 2001; 31(4): 595-601.
6. Lawler JS, Zampini D, Shah SP. Permeability of cracked hybrid fiber-reinforced mortar under load. *ACI Materials Journal* 2002; 99(4): 379-385.
7. Sorelli LG, Meda A, Plizzari GA. Bending and uniaxial tensile tests on concrete reinforced with hybrid steel fibers. *J. Mat. Civ. Eng* 2005; 17(5): 519-527.
8. Markovic, I. High-performance hybrid-fibre concrete: development and utilisation. Ph.D. Thesis, Delft University of Technology, Netherlands, 2006.
9. Banthia N, and Sappakittipakorn M. Toughness enhancement in steel fiber reinforced concrete through fiber hybridization. *Cement and Concrete Research* 2007; 37(9): 1366-1372.

10. Stähli, P., and Van Mier, J. G. Manufacturing, fibre anisotropy and fracture of hybrid fibre concrete. *Engineering Fracture Mechanics* 2007; 74(1-2): 223-242.
11. Akcay B, and Tasdemir MA. Mechanical behaviour and fibre dispersion of hybrid steel fibre reinforced self-compacting concrete. *Construction and Building Materials* 2012; 28(1): 287-293.
12. Akcay B. Experimental investigation on uniaxial tensile strength of hybrid fibre concrete. *Composites Part B: Engineering* 2012; 43(2): 766-778.
13. Kim DJ, Park SH, Ryu GS, Koh KT. Comparative flexural behavior of hybrid ultra high performance fiber reinforced concrete with different macro fibers. *Construction and Building Materials* 2011; 25(11): 4144-4155.
14. Park SH, Kim DJ, Ryu GS, Koh KT. Tensile behavior of ultra high performance hybrid fiber reinforced concrete. *Cement and Concrete Composites* 2012; 34(2): 172-184.
15. Nguyen DL, Kim DJ, Ryu GS, Koh KT. Size effect on flexural behavior of ultra-high-performance hybrid fiber-reinforced concrete. *Composites Part B: Engineering* 2013; 45(1): 1104-1116.
16. Visintin P, Sturm AB, Mohamed Ali MS, Oehlers DJ. Blending macro and micro fibres to enhance the serviceability behaviour of UHPFRC. *Australian Journal of Civil Engineering* 2018; 16(2): 106-121.
17. Fantilli AP., Kwon S, Mihashi H, Nishiwaki T. Synergy assessment in hybrid Ultra-high Performance Fiber-Reinforced Concrete (UHP-FRC). *Cement and Concrete Composites* 2018; 86: 19-29.
18. Chun B, Yoo DY. Hybrid effect of macro and micro steel fibers on the pullout and tensile behaviors of ultra-high-performance concrete. *Composites Part B: Engineering* 2019; 162: 344-360.

19. Voo YL, Foster SJ, Gilbert RI. Shear strength of fiber reinforced reactive powder concrete prestressed girders without stirrups. *Journal of Advanced Concrete Technology* 2006; 4(1): 123-132.
20. Turker K, Hasgul U, Birol T, Yavas A, Yazici H. Hybrid fiber use on flexural behaviour of ultra high performance fiber concrete beams. *Composite Structures* 2019; 229: 1-15.
21. Bachmann H. Influence of shear and bond on rotational capacity of reinforced concrete beams. Bericht Nr. 36, Institut fur Baustatik, ETH Zurich, Switzerland, 1971.
22. Bigaj AJ. Structural dependence of rotation capacity of plastic hinges in RC beams and slabs, Ph.D. Thesis, Delft University of Technology, Netherlands, 1998.
23. Visintin P, Oehlers, DJ. Fundamental mechanics that govern the flexural behaviour of reinforced concrete beams with fibre-reinforced concrete. *Advances in Structural Engineering* 2018, 1369433217739705.
24. Sobuz HR., Visintin P, Mohamed Ali MS, Singh M, Griffith MC, and Sheikh AH. Manufacturing ultra-high performance concrete utilising conventional materials and production methods. *Construction and Building Materials* 2016; 111: 251-261.
25. Sturm AB, Visintin, P. Local bond slip behaviour of steel reinforcing bars embedded in UHPFRC. *Structural Concrete* 2018; 19(2): 508-523.
26. Sturm AB, Visintin P, Farries K, Oehlers DJ. A new testing approach for extracting the shear friction material properties of ultra-high performance fibre reinforced concrete. *J. Mat. Civ. Eng.* 2018; 30(10): 04018235.
27. Standards Australia. Methods of testing concrete-compressive strength tests-concrete, mortar and grout specimens. AS1012.9:2014, Sydney, Australia, 2014.

28. Standards Australia. Methods of testing concrete-Determination of the static chord modulus of elasticity and Poisson's ratio of concrete specimens. AS1012.9:2014, Sydney, Australia, 1997.
29. Standards Australia. Methods of testing concrete-Determination of the drying shrinkage of concrete for samples prepared in the field or in the laboratory. AS1012.13:2015, Sydney, Australia, 2015.
30. Standards Australia. Steel reinforcing materials. AS4671:2001, Sydney, Australia, 2001.
31. Wille K, Naaman AE. Pullout Behavior of High-Strength Steel Fibers Embedded in Ultra-High-Performance Concrete. *ACI Materials Journal* 2012; 109(4): 479-488.
32. Sturm AB, Visintin P, Oehlers DJ. Time-dependent serviceability behavior of reinforced concrete beams: Partial interaction tension stiffening mechanics. *Structural Concrete* 2018; 19(2): 508-523.
33. Hillerborg A. A model for fracture analysis. Report TVBM-3005, Division of Building Materials, Lund Institute of Technology, Lund, Sweden, 1978.
34. Gupta AK, Maestrini SR. Tension-stiffness model for reinforced concrete bars. *Journal of Structural Engineering* 1990; 116(3): 769-790.
35. Wu Z, Yoshikawa H, Tanabe TA. Tension stiffness model for cracked reinforced concrete. *Journal of Structural Engineering* 1991; 117(3): 715-732.
36. Balazs GL. Cracking analysis based on slip and bond stresses. *ACI Materials Journal* 1993; 90: 340-340.
37. Choi CK, Cheung SH. Tension stiffening model for planar reinforced concrete members. *Computers & Structures* 1996; 59(1): 179-190.

38. Sturm AB, Visintin P, Oehlers DJ, Seracino R. Time dependent tension stiffening mechanics of fibre reinforced and ultra-high performance fibre reinforced concrete. *Journal of Structural Engineering* 2018; 144(8): 04018122.
39. Mohamed Ali MS, Oehlers DJ, Griffith MC. The residual strength of confined concrete. *Advances in Structural Engineering* 2010, 13(4), 603-618.
40. Chen Y, Visintin P, Oehlers DJ, Alengaram UJ. Size-dependent stress-strain model for unconfined concrete. *Journal of Structural Engineering* 2013, 140(4), 04013088.
41. AFGC (Association Francaise de Genie Civil). Betons fibres a ultra-hautes performances- Recommandations [Ultra high performance fibre reinforced-concretes – Recommendations]. Paris, France, 2013.
42. CEN (European Committee for Standardisation). Eurocode 2: Design of concrete structures - Part 1-1: General rules and rules for building. EN 1992-1-1:2004 , Brussels, Belgium, 2004.
43. Shima H, Chou LL, Okamura H. Micro and macro models for bond in reinforced concrete. *Journal of the Faculty of Engineering* 1987 ; 39(2): 133-194.
44. Sigrist V, Marti P. Ductility of structural concrete: A contribution. Proc., Workshop: Development of EN 1992 in Relation to New Research Results and to the CEB-FIP Model Code 1990 211–223. Faculty of Civil Engineering, Czech Technical Univ, Prague, Czech Republic, 1994.
45. Lowes LN, Moehle JP, Govindjee S. Concrete-Steel Bond Model for Use in Finite Element Modeling of Reinforced Concrete Structures. *ACI Structural Journal* 2004; 101(4): 501-511.
46. Ruiz MF, Muttoni A, Gambarova PG. Analytical modeling of the pre-and postyield behavior of bond in reinforced concrete. *Journal of Structural Engineering* 2007; 133(10): 1364-1372.

47. Wu HQ, Gilbert RI. Modeling short-term tension stiffening in reinforced concrete prisms using a continuum-based finite element model. *Engineering Structures* 2009; 31(10): 2380-2391.
48. fib (International Federation for Structural Concrete) fib Model Code for Concrete Structures 2010. Ernst & Sohn, Berlin, Germany, 2013.
49. Santos J, and Henriques AA. New finite element to model bond–slip with steel strain effect for the analysis of reinforced concrete structures. *Engineering Structures* 2015; 86: 72-83.
50. Zhou B, Wu R, Feng J. Two models for evaluating the bond behavior in pre-and post-yield phases of reinforced concrete. *Construction and Building Materials* 2017, 147, 847-857.
51. Malek A, Scott A, Pampanin S, Hoult NA. Postyield Bond Deterioration and Damage Assessment of RC Beams Using Distributed Fiber-Optic Strain Sensing System. *Journal of Structural Engineering* 2019; 145(4): 04019007.
52. Tanigawa Y, Yamada K, Hatanaka S. Stress-Strain Behavior of Steel Fiber Reinforced Concrete Subjected to Compressive Load. Research Report Faculty of Engineering, Mie University, 6, 93-106, 1981.
53. Stengel T, and Schießl P.. Life cycle assessment (LCA) of ultra high performance concrete (UHPC) structures. *Eco-efficient Construction and Building Materials* 2014: 528-564.